RAA 2017 Vol. **17** No. **10**, 105 (16pp) doi: 10.1088/1674–4527/17/10/105

http://www.raa-journal.org *http://iopscience.iop.org/raa*

***R**esearch in*
***A**stronomy and*
***A**strophysics*

Radio stars observed in the LAMOST spectral survey

Li-Yun Zhang[1], Qiang Yue[1], Hong-Peng Lu[1], Xian-Ming L. Han[1,2], Yong Zhang[3], Jian-Rong Shi[4], Yue-Fei Wang[3], Yong-Hui Hou[3] and Zi-Huang Cao[4]

[1] College of Physics/Department of Physics and Astronomy, Guizhou University, Guiyang 550025, China; *liy_zhang@hotmail.com*
[2] Department of Physics and Astronomy, Butler University, Indianapolis, IN 46208, USA
[3] Nanjing Institute of Astronomical Optics & Technology, National Astronomical Observatories, Chinese Academy of Sciences, Nanjing 210042, China
[4] Key Laboratory of Optical Astronomy, National Astronomical Observatories, Chinese Academy of Sciences, Beijing 100012, China

Received 2017 January 16; accepted 2017 June 17

Abstract Radio stars have attracted astronomers' attention for several decades. To better understand the physics behind stellar radio emissions, it is important to study their optical behaviors. The LAMOST survey provides a large database for researching stellar spectroscopic properties of radio stars. In this work, we concentrate on their spectroscopic properties and infer physical properties from their spectra, such as stellar activity and variability. We mined big data from the LAMOST spectral survey Data Release 2 (DR2), published on 2016 June 30, by cross-matching them with radio stars from FIRST and other surveys. We obtained 783 good stellar spectra with high signal to noise ratio for 659 stars. The criteria for selection were positional coincidence within $1.5''$ and LAMOST objects classified as stars. We calculated the equivalent widths (EWs) of the Ca II H&K, Hδ, Hγ, Hβ, Hα and Ca II IRT lines by integrating the line profiles. Using the EWs of the Hα line, we detected 147 active stellar spectra of 89 objects having emissions above the Hα continuum. There were also 36 objects with repeated spectra, 28 of which showed chromospheric activity variability. Furthermore, we found 14 radio stars emitting noticeably in the Ca II IRT lines. The low value of the EW_{8542}/EW_{8498} ratio for these 14 radio stars possibly alludes to chromospheric plage regions.

Key words: stars: chromosphere — stars: activity — stars: radio — stars: spectroscopic

1 INTRODUCTION

Stars are, in general, studied by optical broad-band CCD observations, infrared photometry and spectroscopy as well as X-ray, ultraviolet and radio wavelengths (e.g., Butler et al. 2015; Osten et al. 2006). Late-type stars often display manifestations of magnetic activity such as chromospheric plages and flares, and coronal transition region emissions (e.g., Güdel 2002; Berdyugina 2005; Hall 2008). Radio emission from stellar sources was discovered over the past several decades (e.g., Güdel 2002). Most stellar objects have been identified in optical wavelengths, with radio stars contributing about 0.1 percent of the total stellar population (Flesch 2016). However, a wide variety of non-degenerate radio stars is present in the Hertzsprung-Russell diagram (e.g., Güdel 2002; Paredes 2005). Many different types of stars produce radio emissions (e.g., Wendker 1995; Güdel 2002). Among them there are pre-main sequence stars (Hughes 1988; Carkner et al. 1997), ultracool and brown dwarfs (Berger 2002; Berger et al. 2008), flare stars (White et al. 1989; Osten et al. 2006) and so on.

Wendker (1995) published a catalog of radio stars, which was then updated by Wendker (2015). It includes a total of 3699 stars or binary systems. 821 objects were detected at least once in meter to sub-millimeter wavelengths, and 2192 stars only have upper limits of radio flux. Some statistics on the variability of radio continuum emissions from stars were also provided (Wendker 1987, 1995). The Faint Images of the Radio Sky at Twenty cm (FIRST) survey offers a factor of 50 improvement in ob-

Table 1 Radio Stars Observed with LAMOST

LAMOST name	Date	S/N					Sp	Mtype							Reference
	(d)	u	g	r	i	z	Sp	u	g	r	i	J	H	K	
(1)	(2)	(3)	(4)	(5)	(6)	(7)	(8)	(9)	(10)	(11)	(12)	(13)	(14)	(15)	(16)
J030646.90+240209.1	2013-10-5	9.21	91.4	187.19	263.4	212.76	G5	99	12.47	11.48	0	9.83	9.26	9.13	Wendker 1995
J032858.10+311803.6	2013-12-6	2.16	10.79	28.78	72.38	70.6	M1	99	19.06	16.92	15.65	99	99	99	Wendker 1995
J034743.11+241655.5	2013-1-2	27.72	113.05	194.54	247.8	197.03	F5	99	12.19	11.66	11.28	10.41	10.09	10	Wendker 1995
J040313.95+255259.7	2014-1-30	4.83	36.88	73.77	100.64	77.58	K3	99	99	99	99	10.84	10.32	10.16	Wendker 1995
J040313.95+255259.7	2014-1-30	5.69	42.49	86.64	118.82	93.38	K3	99	99	99	99	10.84	10.32	10.16	Wendker 1995
J040439.37+215818.4	2013-10-26	3.09	26.61	96.13	223.29	233.24	M3	99	15.61	14.22	0	99	99	99	Wendker 1995
J040530.88+215110.5	2013-10-26	2.83	24.49	82.83	178.17	183.59	M1	99	15.66	14.18	12.88	99	99	99	Wendker 1995
J040530.87+215110.6	2013-9-27	1.08	3.01	10.29	30.29	36.76	M3	99	99	99	99	10.95	10.29	10.06	Wendker 1995
J041314.16+281910.4	2014-1-30	1.26	16.33	51.06	129.78	133.71	M3	99	14.3	13.14	0	9.64	8.87	8.63	Wendker 1995
J041314.16+281910.4	2014-1-30	1.39	13.35	42.11	108.85	110.71	M3	99	14.3	13.14	0	9.64	8.87	8.63	Wendker 1995
J041314.14+281910.8	2012-1-22	5.89	72.59	77.73	160.46	158.39	M4	99	99	99	16.8	99	99	99	Wendker 1995
J041414.60+282757.8	2014-1-25	2.44	32.1	95.58	219.91	233.05	M4	99	14.84	13.41	0	9.47	8.67	8.19	Wendker 1995
J041414.60+282757.8	2014-1-25	2.43	32.5	83.64	195.26	208.65	M4	99	14.84	13.41	0	9.47	8.67	8.19	Wendker 1995
J041414.60+282757.8	2014-1-30	1.26	9.27	33.71	94.72	100.07	M4	99	14.84	13.41	0	9.47	8.67	8.19	Wendker 1995
J041417.01+281057.5	2014-1-25	16.93	65.53	138.83	197.81	172.4	K3	99	14.57	13.42	11.41	9.56	8.24	7.13	Wendker 1995
J041417.01+281057.5	2014-1-25	14.47	61.34	146.25	210.96	188.6	K3	99	14.57	13.42	11.41	9.56	8.24	7.13	Wendker 1995
J041430.60+285129.8	2014-1-25	1.17	13.18	36.51	60.38	52.18	M0	99	99	99	99	9.21	8.6	8.36	Wendker 1995
J041447.31+264626.1	2014-1-30	2.16	22.26	78.1	159.77	146.51	M3	99	14.72	13.23	0	9.9	9.18	8.87	Wendker 1995
J041447.31+264626.1	2014-1-30	2.26	20.72	71.63	146.83	134.95	M3	99	14.72	13.23	0	9.9	9.18	8.87	Wendker 1995
J041449.29+281230.2	2013-2-8	1.42	10.5	42.98	138.73	162.08	M4	99	15.81	14.21	0	99	99	99	Wendker 1995
J041449.28+281230.5	2014-1-30	1.9	6.39	29.15	101.29	122.72	M4	99	99	99	99	9.65	8.57	8.12	Wendker 1995
J041449.29+281230.2	2012-1-4	2.47	4.63	16.99	70.43	121.46	M4	99	15.81	14.21	0	99	99	99	Wendker 1995
J041449.28+281230.5	2014-1-25	2.52	7.05	30.77	84.54	97.12	M4	99	99	99	99	9.65	8.57	8.12	Wendker 1995
J041449.29+281230.2	2011-12-18	1.43	11.03	32.67	110.91	132.25	M4	99	15.81	14.21	0	99	99	99	Wendker 1995
J041449.28+281230.5	2014-1-30	2.13	5.36	21.33	78.63	97.81	M4	99	99	99	99	9.65	8.57	8.12	Wendker 1995
J041449.28+281230.5	2014-1-25	2.15	5.4	22.98	62.98	74.2	M4	99	99	99	99	9.65	8.57	8.12	Wendker 1995
J041449.29+281230.2	2012-1-13	2.33	12.65	40.9	135.12	160.99	M4	99	15.81	14.21	0	99	99	99	Wendker 1995
J041447.87+264810.7	2014-1-30	3.04	30.09	96.35	187.72	169.3	M1	99	14.44	13.02	0	9.87	9.05	8.81	Wendker 1995
J041447.87+264810.7	2014-1-30	3.14	31.68	105.94	204.66	183.36	M1	99	14.44	13.02	0	9.87	9.05	8.81	Wendker 1995
J041628.11+280735.0	2014-1-30	2.57	46.41	75.74	135.1	123.85	M0	99	0	12.57	11.62	9.25	8.52	8.32	Wendker 1995
J041628.11+280735.0	2014-1-25	5.47	49.99	113.28	170.27	148.13	M0	99	0	12.57	11.62	9.25	8.52	8.32	Wendker 1995
J041738.94+283300.1	2014-1-25	2.21	36.92	82.02	170.67	156.32	M1	99	14.3	12.97	0	9.98	9.29	9.05	Wendker 1995
J041738.94+283300.1	2014-1-25	2.05	33.01	75	147.49	134.55	M1	99	14.3	12.97	0	9.98	9.29	9.05	Wendker 1995
J041831.12+281628.4	2014-1-30	1.68	3.63	6.89	21.27	25.69	M5	99	15.97	13.81	0	9.83	8.68	7.88	Wendker 1995
J041831.12+281628.4	2014-1-25	7.43	20.37	48.19	84.4	85.23	M6	99	15.97	13.81	0	9.83	8.68	7.88	Wendker 1995
J041831.58+281658.5	2014-1-30	1.31	4.26	9.59	30.76	34.72	M4	99	99	99	99	10.52	9.77	9.36	Wendker 1995
J041831.60+281658.3	2013-2-8	1.18	4.68	19.67	59.07	66.4	M3	99	99	99	14.6	99	99	99	Wendker 1995
J041831.60+281658.3	2012-1-4	1.86	6.28	13.43	31.11	47.75	M4	99	99	99	14.6	99	99	99	Wendker 1995
J041912.81+282933.0	2014-1-25	1.73	3.53	8.07	24.69	28.43	M4	99	99	99	99	10.49	9.7	9.31	Wendker 1995
J041912.80+282932.7	2013-12-31	3.1	19.7	62.99	172.79	186.95	M4	99	15.94	14.81	0	99	99	99	Wendker 1995
J041912.80+282932.7	2012-10-5	1.11	1.91	4.09	33.3	62.5	M4	99	15.94	14.81	0	99	99	99	Wendker 1995
J041915.83+290626.9	2014-1-25	1.35	4.75	5.91	16.34	14.93	M0	99	99	99	99	9.1	8.22	7.74	Wendker 1995
J041926.27+282613.9	2014-1-25	2.34	31.66	80.64	121.8	104.47	K7	99	13.75	12.24	0	9.5	8.65	8.42	Wendker 1995
J041935.45+282721.8	2014-1-25	1.35	1.84	2.66	8.42	11.1	M6	99	99	99	99	10.95	10.37	9.97	Wendker 1995
J041935.46+282721.3	2012-10-5	1.74	2.91	3.63	16.39	30.93	M5	99	99	99	14	99	99	99	Wendker 1995
J041935.46+282721.3	2013-12-31	2.57	13.17	44.03	161.5	185.74	M6	99	99	99	14	99	99	99	Wendker 1995

Notes: (1) We only show some part of the radio stars in Table 1. The parameters of all the radio stars we studied are available in *http://www.raa-journal.org/docs/Supp/ms20170016Table1.txt*. (2) The code 99 means no data. The magnitudes in different bands are from the SDSS (Gunn et al. 1998; York et al. 2000) and 2MASS catalogs (Skrutskie et al. 2006).

servation of the radio sky using the NRAO Very Large Array (VLA) (e.g., Helfand et al. 1999). FIRST corresponds to about 10 575 square degrees of sky coverage. Over most of the FIRST survey area, the detection limit was about 1 mJy. McMahon et al. (2002) published optical counterparts of 70 000 radio objects from the VLA FIRST radio survey. They also discussed the reliability of these identifications vs. optical and radio morphology. Ivezić et al. (2002) also associated 10^5 FIRST core sources with optical counterparts in the Sloan Digital Sky Survey (SDSS) and concluded that the spectra were extremely useful in examining the nature of the targeted sources. Kimball et al. (2009) chose 112 candidate radio stars from the FIRST and SDSS surveys, and analyzed their magnetic activities. Recently, the VLA FIRST project published a final catalog of 946 432 objects and their identifications are at the FIRST survey's website (Helfand et al. 2015).

Berger (2006) made radio observations of 90 dwarf stars and brown dwarfs of spectral types M5–T8 and discussed the distribution of magnetic field strengths. A few years later, Berger et al. (2008) obtained the first simultaneous radio, X-ray and Hα observations of ultra-cool dwarfs to study stellar magnetic activity and its relationship with chromospheric and coronal emissions. They analyzed about 100 late M and L dwarfs from VLA observations to explore the rotation-activity relationship (McLean et al. 2012). Flesch (2010) published a catalog by combining the radio and X-ray objects associated with optical objects. Later, they revised the catalog (Flesch & Hardcastle 2004).

Karoff et al. (2016) analyzed the LAMOST spectroscopic data of 5648 solar-like stars (including 48 superflare stars) and estimated the relationship between chromospheric activity and the occurrence of superflares. Frasca et al. (2016) studied LAMOST spectra of spectroscopic follow-up observations from the Kepler survey by means of the spectral subtraction of inactive templates using the code ROTFIT and determined the stellar parameters. Based on the chromospheric activity indicators Hα and Ca II IRT lines, they found 442 chromospherically active stars and determined the relationship between these chromospheric fluxes and the precise rotation periods from Kepler photometry (Frasca et al. 2016).

The Large Sky Area Multi-Object Fiber Spectroscopic Telescope (LAMOST) offers data to study chromospheric activity of radio stars. We present a catalog of radio stars observed in the LAMOST survey, and discuss properties of their chromospheric activity in the Hα, Hβ, Hγ, Hδ, Ca II H & K and Ca II IRT lines.

2 DATA

LAMOST is a reflecting Schmidt optical telescope located at Xinglong Station of National Astronomical Observatories, Chinese Academy of Sciences (NAOC), and is designed to make stellar and extra-galactic spectroscopic surveys. Its effective aperture is between 3.6 m and 4.9 m and the field of view is about 5° wide (Wang et al. 1996). It can obtain spectra of up to 4000 objects in a single exposure (e.g., Cui et al. 2012; Zhao et al. 2012; Luo et al. 2015). Specialists associated with LAMOST developed reliable automated methods and softwares (the LAMOST stellar parameter pipeline) to measure stellar fundamental parameters of the LAMOST spectroscopic survey (the effective temperature, surface gravity and metallicity) (Wu et al. 2011, 2014). The stellar spectra of 3.84 million LAMOST stellar objects were published on 2016 June 30 in the LAMOST Data Release 2 (DR2). These stellar spectra carry valuable information that can be used for the study of chromospheric activity and variability of radio stars. We cross-matched radio stars in the FIRST catalog and from other radio surveys (e.g., McMahon et al. 2002; Helfand et al. 2015; McLean et al. 2012; Wendker 1995; Flesch 2010) with the subsample of stellar sources in the LAMOST DR2 catalog, and obtained 783 stellar spectra with a signal to noise ratio (S/N) greater than about 8, which correspond to 659 individual targets.

In Table 1 we list these sources along with the LAMOST name (Col. (1)), observation date (Col. (2)), the S/N in Sloan $ugriz$ bands (from Col. (3) to Col. (7)), spectral type (Col. (8)), magnitudes in $ugrizJHK$ bands (Col. (9) to Col. (15)), and the references of radio stars (Col. (16)) in Table 1. We publish all the data in the online version of the journal.

3 SPECTROSCOPIC ANALYSES

We calculated the equivalent widths (EWs) of the spectral lines using the usual formula

$$\mathrm{EW} = \int_{\mathrm{line}} \frac{F_\lambda - F_C}{F_C} d\lambda,$$

where F_λ is the line flux and F_C is that at the continuum. With this definition, emission lines have a positive EW. The spectral regions for evaluating the continuum at the two sides of each line are 6555–6560 Å and 6570–6575 Å for Hα; 4840.0–4850.0 Å and 4875.0–4885.0 Å for Hβ, 4310.0–4330.0 Å and 4350.0–4370.0 Å for Hγ; 4075.0–4095.0 Å and 4110.0–4130.0 Å for Hδ; and 3952.8–3956.0 Å and 3974.0–3976.0 Å for Ca II K, respectively. These wavelength intervals are close to

Table 2 EWs of Chromospheric Emission Lines for 89 Radio Stars

No.	Name	Sp	Re	Name	6cm	kHz	Flux	V1	Hα	V2	Hβ	Hγ	Hδ	Ca IIH	Ca IIK
(1)	(2)	(3)	(4)	(5)	(6)	(7)	(8)	(9)	(10)	(11)	(12)	(13)	(14)	(15)	(16)
1	J032858.10+311803.6	M2	[1]	107HH 12		230	38.0	-	11.827 ± – 0.223	-	6.245 ± 0.201	4.200 ± 0.131	±	±	±
2	J040439.37+215818.4	M3	[1]	HBC 360	0.6			-	5.450 ± 0.228	-	6.673 ± 0.221	5.019 ± 0.071	5.386 ± 0.376	16.289 ± 0.06	14.425 ± 0.365
3	J040530.88+215110.5	M3	[1]	HBC 362	0.6			-	6.931 ± 0.171	v	7.676 ± 0.019	6.305 ± 0.367	6.766 ± 0.557	20.438 ± 0.19	22.120 ± 1.15
3	J040530.87+215110.6	M2	[1]	HBC 362	0.6			-	12.186 ± 0.774	v	9.359 ± 0.449	10.360 ± 7.417	±	38.379 ± 2.36	±
4	J041314.16+281910.4	M2	[1]	HBC 365	0.6			-	2.116 ± 0.16	v	1.341 ± 0.118	±	±	9.878 ± 0.272	9.981 ± 0.729
4	J041314.16+281910.4	M3	[1]	HBC 365	0.6			-	3.133 ± 0.162	v	2.615 ± 0.078	1.208 ± 0.042	±	10.916 ± 0.384	19.218 ± 0.208
4	J041314.14+281910.8	M3	[1]	HBC 365	0.6			-	3.265 ± 0.338	v	2.472 ± 0.037	0.879 ± 0.04	±	15.317 ± 1.42	18.765 ± 1.505
5	J041414.60+282757.8	M3	[1]	FN Tau	75.0	230	31.0	-	18.444 ± 0.646	v	11.906 ± 0.016	9.399 ± 0.082	9.072 ± 0.072	27.762 ± 1.79	28.230 ± 0.32
5	J041414.60+282757.8	M4	[1]	FN Tau	75.0	230	31.0	-	17.433 ± 0.397	v	9.099 ± 0.207	8.102 ± 0.081	±	±	±
5	J041414.60+282757.8	M3	[1]	FN Tau	75.0	230	31.0	-	13.844 ± 0.316	v	8.683 ± 0.15	8.013 ± 0.123	7.658 ± 0.064	23.080 ± 2.46	18.306 ± 1.244
6	J041417.01+281057.5	K5	[1]	CW Tau	0.30	230	96.0	-	222.945 ± 1.855	v	41.770 ± 2.61	25.284 ± 3.496	18.667 ± 0.057	54.338 ± 8.142	76.067 ± 1.617
6	J041417.01+281057.5	K5	[1]	CW Tau	0.30	230	96.0	-	87.379 ± 6.671	v	12.457 ± 1.153	±	±	±	±
6	J041417.01+281057.5	K5	[1]	CW Tau	0.30	230	96.0	-	247.056 ± 5.244	v	44.394 ± 1.566	18.490 ± 1.65	11.051 ± 0.249	39.122 ± 4.298	48.512 ± 2.378
6	J041417.01+281057.5	K5	[1]	CW Tau	0.30	230	96.0	-	80.762 ± 1.228	v	12.604 ± 1.056	±	±	8.097 ± 0.58	19.073 ± 0.537
7	J041430.60+285129.8	K7	[1]	LkCa 2	0.6			-	1.433 ± 0.074	-	±	±	±	±	±
8	J041447.31+264626.1	M3	[1]	FP Tau		230	50.0	-	46.160 ± 0.96	v	14.838 ± 0.278	15.869 ± 2.119	12.347 ± 0.127	19.700 ± 1.23	8.361 ± 0.061
8	J041447.31+264626.1	M2	[1]	FP Tau		230	50.0	-	54.556 ± 3.846	v	13.228 ± 0.048	14.698 ± 1.798	17.314 ± 1.614	26.452 ± 0.902	10.395 ± 0.045
9	J041449.29+281230.2	M2	[1]	FO Tau		230	50.0	-	114.281 ± 3.481	v	55.119 ± 2.231	43.856 ± 3.626	41.780 ± 1.17	94.798 ± 2.21	84.371 ± 1.429
9	J041449.28+281230.5	M4	[1]	FO Tau		230	50.0	-	121.209 ± 4.291	v	79.030 ± 3.58	31.071 ± 1.029	23.052 ± 0.152	25.238 ± 0.392	18.452 ± 1.328
9	J041449.29+281230.2	M5	[1]	FO Tau		230	50.0	-	135.805 ± 14.695	v	170.04 ± 33.44	282.39 ± 51.99	101.98 ± 41.33	234.33 ± 167.9	167.28 ± 53.53
9	J041449.28+281230.5	M4	[1]	FO Tau		230	50.0	-	127.529 ± 8.071	v	72.666 ± 4.094	49.071 ± 0.299	37.048 ± 0.748	54.500 ± 2.66	53.433 ± 1.343
9	J041449.29+281230.2	M4	[1]	FO Tau		230	50.0	-	130.805 ± 1.595	v	66.829 ± 4.209	53.685 ± 4.805	55.888 ± 7.488	100.228 ± 1.58	93.888 ± 26.912
9	J041449.28+281230.5	M4	[1]	FO Tau		230	50.0	-	132.381 ± 1.281	v	67.971 ± 0.029	25.734 ± 0.596	19.374 ± 0.186	21.534 ± 0.896	15.899 ± 0.821
9	J041449.28+281230.5	M3	[1]	FO Tau		230	50.0	-	120.660 ± 0.76	v	72.939 ± 3.399	48.004 ± 0.314	36.778 ± 1.218	43.150 ± 38.948	41.548 ± 4.222
9	J041449.29+281230.2	M4	[1]	FO Tau		230	50.0	-	113.665 ± 5.865	v	69.514 ± 2.924	51.335 ± 2.565	45.608 ± 0.342	87.798 ± 9.53	65.534 ± 3.604
10	J041447.87+264810.7	M2	[1]	CX Tau		230	40.0	-	34.289 ± 1.079	v	14.527 ± 0.467	14.483 ± 1.653	1.234 ± 11.846	21.396 ± 0.214	7.219 ± 0.83
10	J041447.87+264810.7	M2	[1]	CX Tau		230	40.0	-	27.862 ± 0.998	v	15.487 ± 0.897	17.394 ± 3.324	±	16.131 ± 1.079	7.303 ± 0.76
11	J041628.11+280735.0	K7	[1]	DM+10551	0.6			-	4.108 ± 0.08	v	1.483 ± 0.138	±	±	11.007 ± 0.283	12.597 ± 0.323
11	J041628.11+280735.0	K5	[1]	DM+10551	0.6			-	4.836 ± 0.035	v	1.934 ± 0.04	±	±	13.657 ± 1.15	15.203 ± 0.273
12	J041738.94+283300.1	M2	[1]	HBC 371	0.5			-	3.772 ± 0.178	n	2.349 ± 0.089	1.643 ± 0.114	1.658 ± 0.153	12.747 ± 0.333	16.889 ± 1.131
12	J041738.94+283300.1	M2	[1]	HBC 371	0.5			-	3.860 ± 0.042	n	2.374 ± 0.172	±	±	16.701 ± 0.499	18.438 ± 1.552
13	J041831.12+281628.4	M3	[1]	DD Tau	0.5	230	50.0	-	300.448 ± 15.252	v	43.136 ± 0.406	27.009 ± 3.429	13.576 ± 1.236	13.695 ± 0.485	±
13	J041831.12+281628.4	M2	[1]	DD Tau	0.5	230	50.0	-	264.300 ± 17.1	v	54.286 ± 5.596	34.478 ± 6.778	23.456 ± 0.256	44.289 ± 7.049	29.528 ± 0.802
14	J041831.58+281658.5	M3	[1]	CZ Tau	0.5			-	4.217 ± 0.142	v	±	±	±	±	±
14	J041831.60+281658.3	M3	[1]	CZ Tau	0.5			-	5.021 ± 0.085	v	±	±	±	±	±
14	J041831.60+281658.3	M4	[1]	CZ Tau	0.5			-	6.048 ± 0.004	v	3.867 ± 0.345	4.725 ± 0.108	±	10.755 ± 0.22	17.511 ± 0.909
15	J041912.81+282933.0	M3	[1]	FQ Tau		230	40.0	-	5.343 ± 0.073	v	55.969 ± 3.319	23.100 ± 0.23	9.380 ± 1.99	57.464 ± 5.59	53.208 ± 5.358
15	J041912.80+282932.7	M4	[1]	FQ Tau		230	40.0	-	51.128 ± 1.292	v	31.753 ± 1.003	19.347 ± 0.193	17.039 ± 0.031	31.210 ± 0.89	31.312 ± 0.528
15	J041912.80+282932.7	M6	[1]	FQ Tau		230	40.0	-	77.950 ± 6.14	v	86.059 ± 4.419	55.317 ± 2.843	100.847 ± 7.153	177.328 ± 60.08	67.410 ± 9.37
16	J041915.83+290626.9	M0	[1]	BP Tau		15	9.0	-	135.743 ± 5.157	v	26.127 ± 1.947	16.389 ± 0.329	±	±	±
16	J041915.83+290626.9	M1	[1]	BP Tau		15	9.0	-	124.073 ± 9.173	v	23.195 ± 0.425	19.951 ± 2.871	±	±	±
17	J041926.27+282613.9	M0	[1]	V819 Tau		230	34.0	v	3.367 ± 0.022	-	±	±	±	±	±
18	J041935.46+282721.4	M6	[1]	FR Tau		230	50.0	-	139.111 ± 7.411	v	34.176 ± 0.436	21.649 ± 0.641	17.210 ± 0.8	19.022 ± 3.74	10.355 ± 0.225
18	J041935.45+282721.8	M5	[1]	FR Tau		230	50.0	-	32.268 ± 0.932	v	±	±	±	±	±
18	J041935.46+282721.3	M6	[1]	FR Tau		230	50.0	-	77.453 ± 2.067	v	10.83 ± 0.31	12.307 ± 0.967	±	±	±
18	J041935.46+282721.3	M6	[1]	FR Tau		230	50.0	-	67.614 ± 4.196	v	66.730 ± 2.18	58.261 ± 1.409	36.353 ± 0.137	73.331 ± 5.04	52.204 ± 0.066
19	J042155.63+275506.0	M0	[1]	DE Tau	0.58			-	80.984 ± 1.344	-	44.363 ± 1.567	26.962 ± 1.328	32.234 ± 3.176	102.723 ± 11.33	93.660 ± 3.88

Notes: [1] Wendker 1995; [2] Helfand et al. 2015; [3] McLean et al. 2012; [4] Berger et al. 2008; [5] Helfand et al. 1999; [6] McMahon et al. 2002; [7] Flesch 2010; [8] Helfand et al. 2015 We only show some part of the radio stars in Table 2. No value with ± means there is no data point. The parameters of all radio stars are available in *http://www.raa-journal.org/docs/Supp/ms20170016Table2.txt.*

those by Hilton et al. (2010) and West et al. (2004, 2011) for the analyses of SDSS spectra. To select radio stars with a high activity level, we used the criteria for the Hα line similar to those of West et al. (2011) and Yi et al. (2014). The EWs of the Hα line are larger than 0 Å for OBAFGK stars (for M stars, they are larger than 0.75 Å), and are simultaneously larger than their uncertainties, whereas the height of the Hα emission must be at least 3 times its noise (e.g., Hawley et al. 2002; Zhang et al. 2016).

We also visually inspected all candidates for active radio stars and manually checked their chromospheric

Table 3 EWs of Ca_{II} IRT Lines for 14 Radio Stars

No.	Name	Sp	Source	Name	$Ca_{II}8498$	$Ca_{II}8542$	$Ca_{II}8662$	EW_{8542}/EW_{8498}
(1)	(2)	(3)	(4)	(5)	(6)	(7)	(8)	(9)
6	J041417.01+281057.5	K5	Wendker 1995	CW Tau	7.120 ± 0.18	12.808 ± 0.102	10.479 ± 0.099	1.799 ± 0.007
6	J041417.01+281057.5	K5	Wendker 1995	CW Tau	4.713 ± 0.007	6.829 ± 0.248	5.819 ± 0.169	1.449 ± 0.052
6	J041417.01+281057.5	K5	Wendker 1995	CW Tau	8.691 ± 0.091	13.395 ± 0.635	9.976 ± 0.094	1.541 ± 0.069
6	J041417.01+281057.5	K5	Wendker 1995	CW Tau	4.270 ± 0.01	7.222 ± 0.218	5.837 ± 1.899	1.691 ± 0.050
9	J041449.29+281230.2	M2	Wendker 1995	FO Tau	2.913 ± 0.097	3.595 ± 0.035	2.904 ± 0.025	1.234 ± 0.010
9	J041449.28+281230.5	M4	Wendker 1995	FO Tau	2.415 ± 0.325	2.542 ± 0.079	3.050 ± 0.143	1.053 ± 0.089
9	J041449.29+281230.2	M5	Wendker 1995	FO Tau	1.160 ± 0.11	1.564 ± 0.076	1.239 ± 0.015	1.348 ± 0.013
9	J041449.28+281230.5	M4	Wendker 1995	FO Tau	3.160 ± 0.09	4.118 ± 0.12	3.006 ± 0.011	1.303 ± 0.021
9	J041449.29+281230.2	M4	Wendker 1995	FO Tau	3.478 ± 0.078	4.207 ± 0.149	3.593 ± 0.07	1.210 ± 0.028
9	J041449.28+281230.5	M4	Wendker 1995	FO Tau	3.142 ± 0.078	3.641 ± 0.066	2.855 ± 0.034	1.159 ± 0.003
9	J041449.28+281230.5	M3	Wendker 1995	FO Tau	3.474 ± 0.054	4.039 ± 0.029	3.399 ± 0.056	1.163 ± 0.003
9	J041449.29+281230.2	M4	Wendker 1995	FO Tau	2.366 ± 0.096	3.268 ± 0.03	1.854 ± 0.176	1.381 ± 0.009
13	J041831.12+281628.4	M3	Wendker 1995	DD Tau	±	±	±	– ± –
13	J041831.12+281628.4	M2	Wendker 1995	DD Tau	8.336 ± 0.484	10.480 ± 0.14	8.860 ± 0.209	1.257 ± 0.020
15	J041912.81+282933.0	M3	Wendker 1995	FQ Tau	7.345 ± 0.395	8.722 ± 0.392	8.378 ± 0.048	1.187 ± 0.015
15	J041912.80+282932.7	M4	Wendker 1995	FQ Tau	±	±	±	– ± –
15	J041912.80+282932.7	M6	Wendker 1995	FQ Tau	4.852 ± 0.172	4.386 ± 0.087	3.778 ± 0.062	0.904 ± 0.025
19	J042155.63+275506.0	M0	Wendker 1995	DE Tau	6.827 ± 0.363	9.357 ± 0.196	8.080 ± 0.105	1.371 ± 0.001
23	J042923.73+243300.2	F4	Wendker 1995	GV Tau	19.447 ± 0.783	16.384 ± 0.616	16.227 ± 0.343	0.842 ± 0.025
23	J042923.73+243300.2	K4	Wendker 1995	GV Tau	17.890 ± 0.13	15.515 ± 0.435	16.198 ± 0.238	0.867 ± 0.015
31	J043138.47+181357.9	M0	Wendker 1995	HL Tau	25.185 ± 0.325	26.262 ± 1.192	17.327 ± 0.127	1.043 ± 0.035
34	J043215.40+242859.7	M0	Wendker 1995	V 806 Tau	1.909 ± 0.055	1.525 ± 0.027	1.534 ± 0.108	0.799 ± 0.031
34	J043215.40+242859.7	M0	Wendker 1995	V 806 Tau	3.053 ± 0.047	2.357 ± 0.059	2.456 ± 0.023	0.772 ± 0.007
41	J043828.58+261049.2	CV	Wendker 1995	DO Tau	356.181 ± 14.281	438.184 ± 261.616	±	1.230 ± 0.708
43	J043920.92+254501.8	M2	Wendker 1995	GN Tau	10.959 ± 0.731	13.390 ± 0.63	12.523 ± 0.017	1.222 ± 0.013
43	J043920.90+254502.1	M1	Wendker 1995	GN Tau	7.996 ± 0.671	3.078 ± 0.138	3.232 ± 0.365	0.385 ± 0.549
44	J043917.42+224753.2	K7	Wendker 1995	VY Tau	2.984 ± 0.065	2.523 ± 0.05	2.218 ± 0.076	0.846 ± 0.014
44	J043917.42+224753.2	K7	Wendker 1995	VY Tau	3.594 ± 0.035	2.895 ± 0.031	2.154 ± 0.731	0.806 ± 0.006
47	J044237.69+251537.0	K7	Wendker 1995	DP Tau	10.873 ± 0.527	9.428 ± 0.534	8.552 ± 0.198	0.867 ± 0.015
49	J045209.70+303745.1	CV	Wendker 1995	Haro 6-39	12.240± 0.43	11.484 ± 0.306	7.981 ± 0.404	0.938 ± 0.015
52	J061250.35-061311.4	CV	Wendker 1995	HH 1-2	50.221± 2.279	61.926 ± 1.316	41.578 ± 1.872	1.233 ± 0.004

Note: No value with ± means there is no data point.

activity spectral lines. The uncertainties in spectral types of the LAMOST observations arise from two subtypes (e.g., Yi et al. 2014; Zhang et al. 2016) with respect to the model of a standard star. We normalized the LAMOST spectra of OBAFGK stars to their continuum by a polynomial fit using the continuum package in the IRAF software[1]. We plotted the LAMOST observed (left panels) and their normalized continuum spectra (right panels) in Figure 1.

We report the LAMOST names of radio stars observed in the LAMOST spectral survey below the panels in Figure 1. At the top of the panels, there is the spectroscopic name from the LAMOST survey, for example, spec-56683-VB063N29V1_sp07-206.fits. We also marked the spectral types of the radio stars and the different chromospheric activity indicators in the figure. We calculated the EWs by integrating over the emission profile using the SPLOT task in the IRAF package. The methods for calculating the EWs and their uncertainties were similar to those of Zhang & Gu (2008). Using the EWs of the Hα line, we detected 147 active spectra of 89 objects with emissions above the continuum. These are listed in Table 2.

In this table we quote the number (Col. (1)), the LAMOST name (Col. (2)), spectral type (Col. (3)), the sources of radio stars (Col. (4)) other name (Col. (5)), radio flux of 6 cm and other radio wavelengths (Col. (6) to Col. (8)), the variation in the radio wavelength (Col. (9)), EWs of Hα (Col. (10)), the flag for variation of chromospheric activity (Col. (11)), Hβ, Hγ, Hδ and Ca II

[1] IRAF is distributed by the National Optical Astronomy Observatories, which are operated by the Association of Universities for Research in Astronomy, Inc., under cooperative agreement with the National Science Foundation.

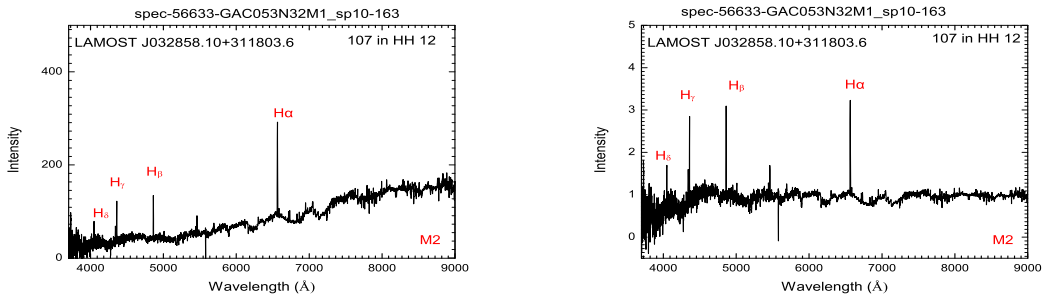

(a) LAMOST J032858.10+311803.6

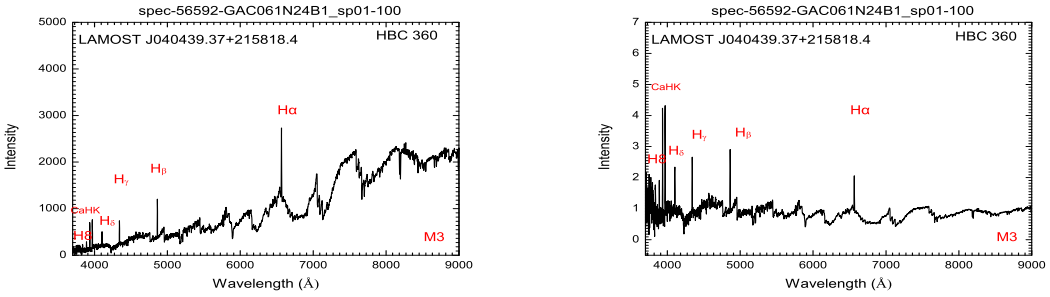

(b) LAMOST J040439.37+215818.4

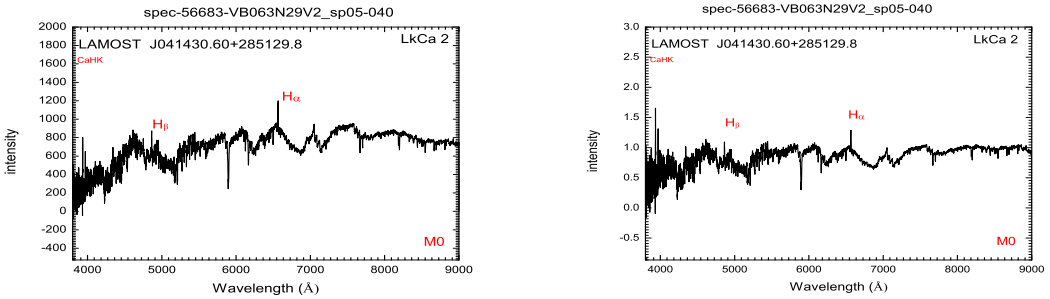

(c) LAMOST J041430.60+285129.8

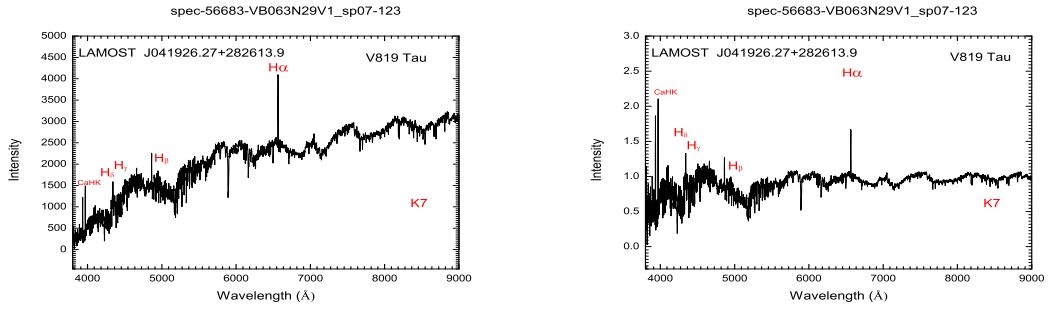

(d) LAMOST J041926.27+282613.9

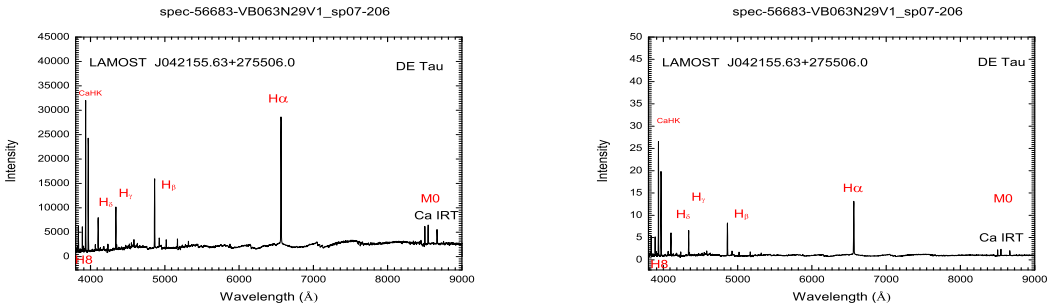

(e) LAMOST J042155.63+275506.0

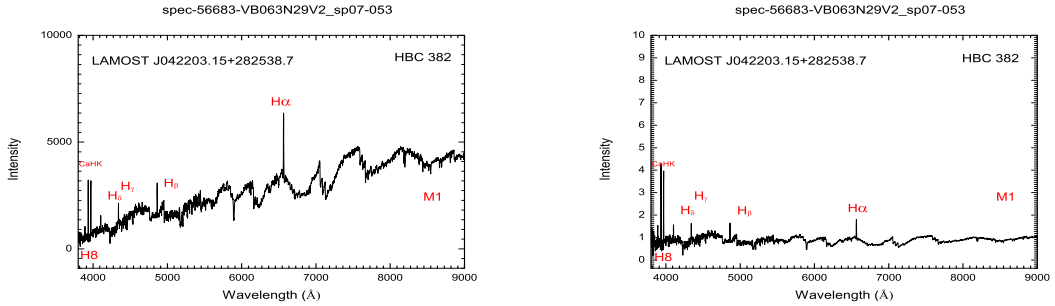

(f) LAMOST J042203.15+282538.7

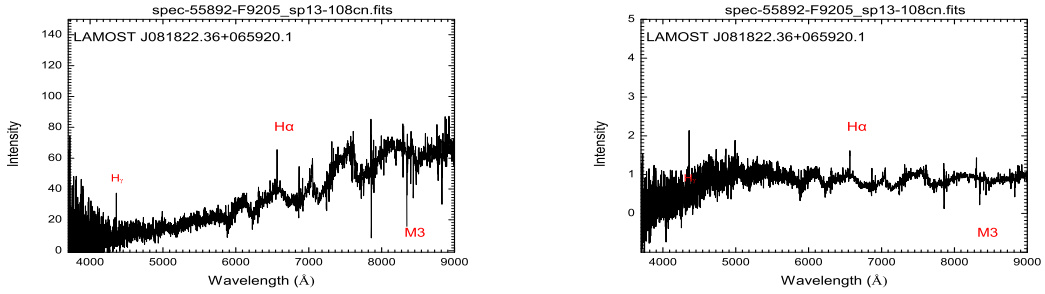

(g) LAMOST J081822.36+065920.1

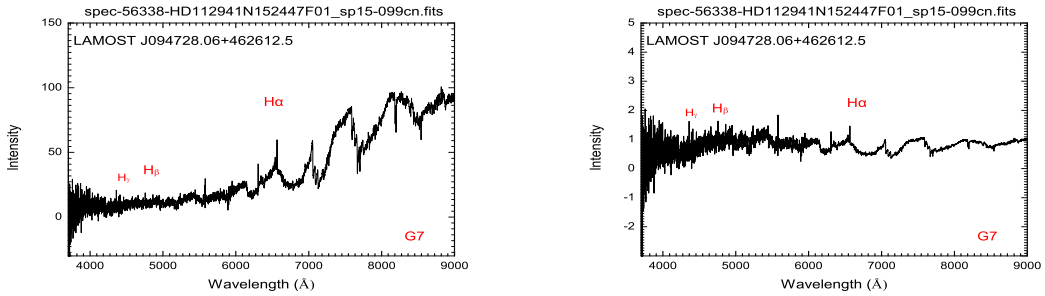

(h) LAMOST J094728.06+462612.5

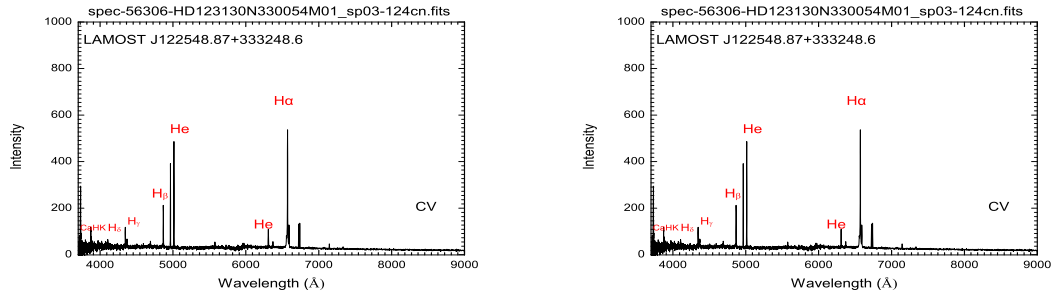

(i) LAMOST J122548.87+333248.6

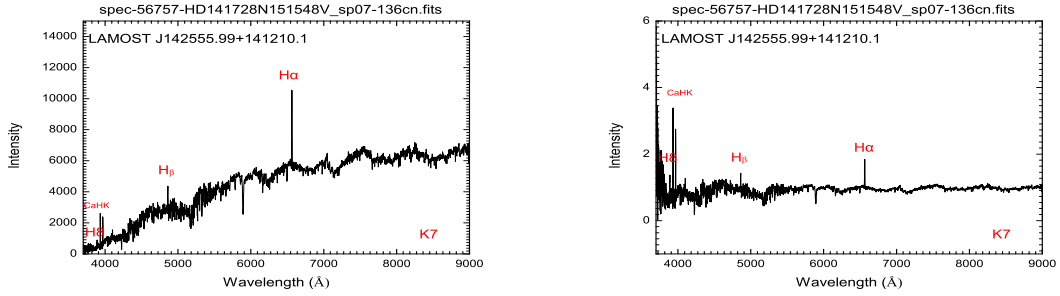

(j) LAMOST J142555.99+141210.1

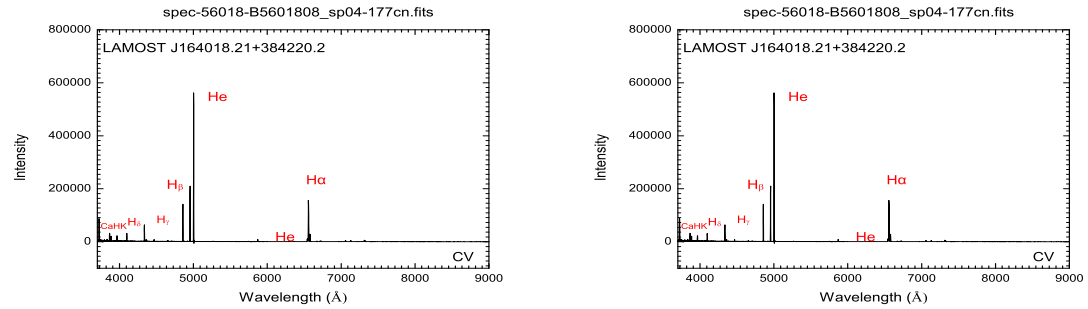

(k) LAMOST J164018.21+384220.2

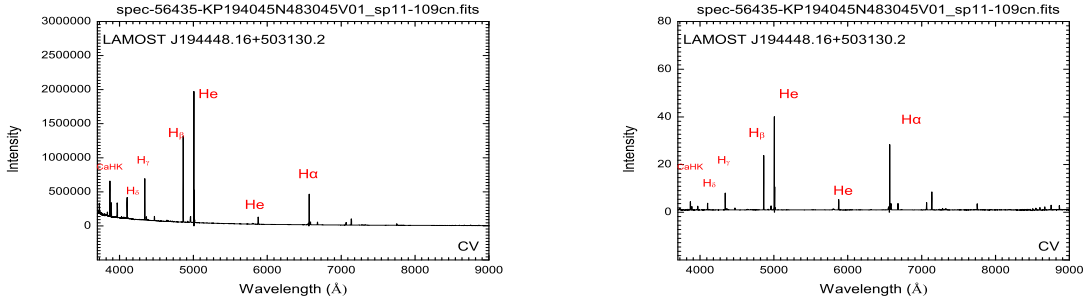

(l) LAMOST J194448.16+503130.2

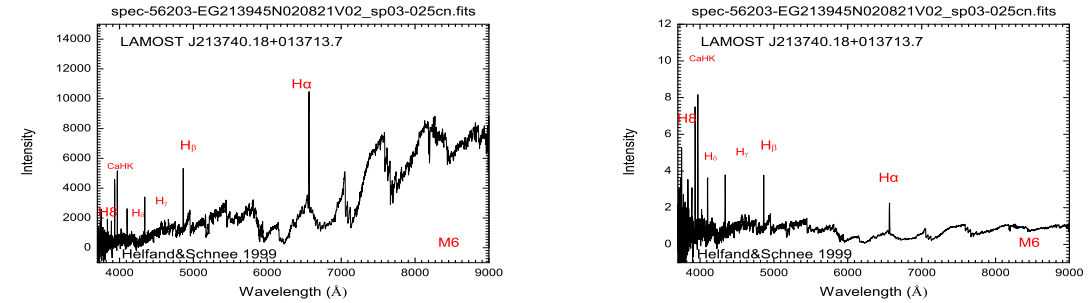

(m) LAMOST J213740.18+013713.7

Fig. 1 Examples of LAMOST spectra (*left*) and their continuum normalized spectra (*right*) for radio stars. Some of them show obvious emissions in the Ca II H&K, Hδ, Hγ, Hβ, Hα and Ca II IRT lines.

H&K lines (Col. (12) to Col. (16)). The printed version of Table 2 displays only a few lines as examples, but the full data set in Table 2 is available in the online version of the journal and can be downloaded as an electronic table from the on-line database at *http://www.raa-journal.org/docs/Supp/ms20170016Table2.txt*.

4 DISCUSSION AND CONCLUSIONS

We studied the chromospheric activity of radio stars using different chromospheric activity indicators, and discussed the statistical properties of chromospheric variability.

4.1 Chromospheric Activity Emission and Variability

Using the EWs of the Hα line, we detected 147 active spectra of 89 objects with emissions above the Hα continuum. There are 34 objects with repeated LAMOST observations. Many of our objects are T Tauri (T Tau) stars in the Tau-Aur complex (e.g., Fernandez et al. 1995; Kenyon & Hartmann 1995; Mohanty et al. 2005; Nguyen et al. 2012). The spectral characteristics (the emission of Hα lines and other spectral lines) of many of the T Tau stars that correspond to our LAMOST objects are consistent with previous low or high-resolution spectra in

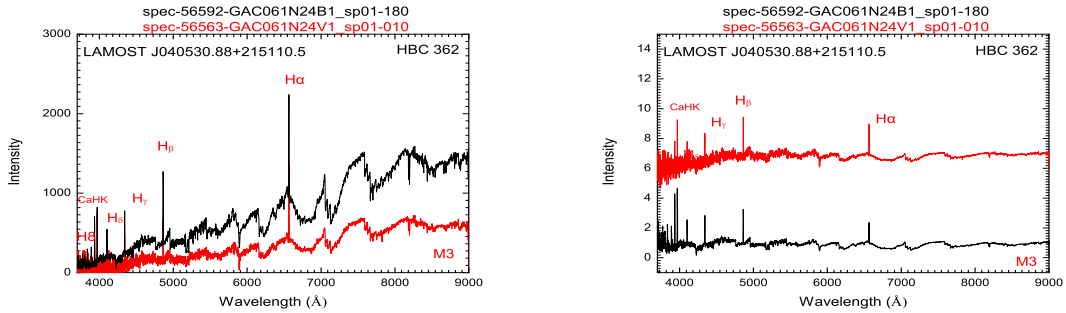

(a) LAMOST J040530.88+215110.5

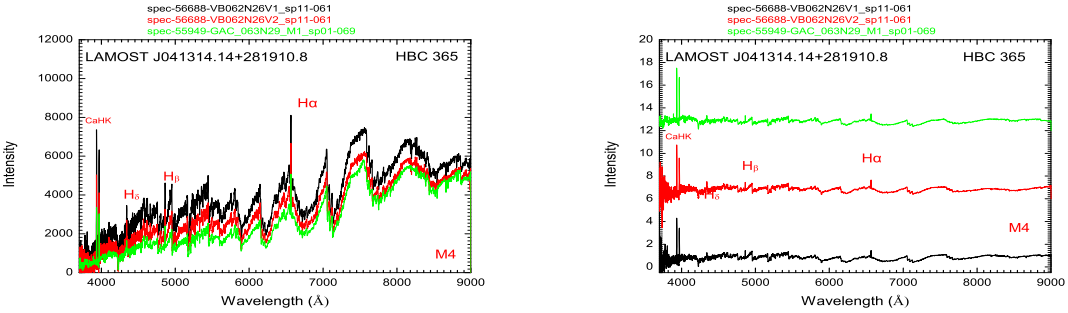

(b) LAMOST J041314.14+281910.8

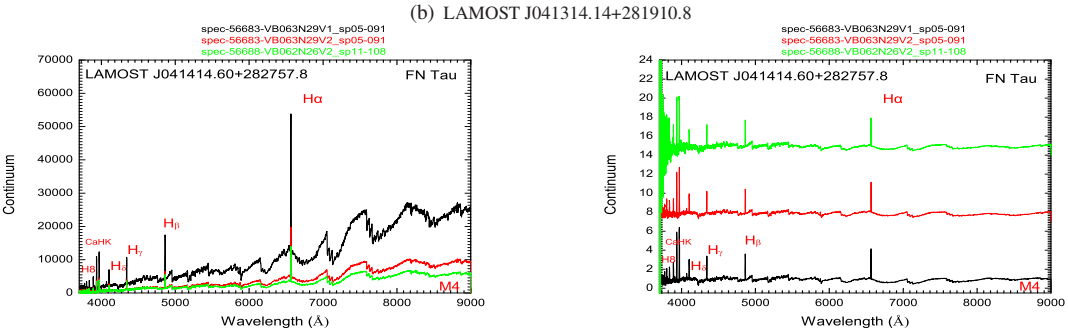

(c) LAMOST J041414.60+282757.8

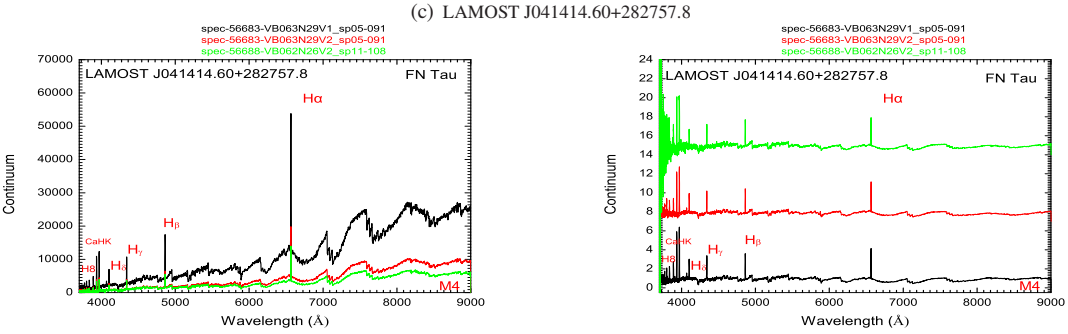

(d) LAMOST J041417.01+281057.5

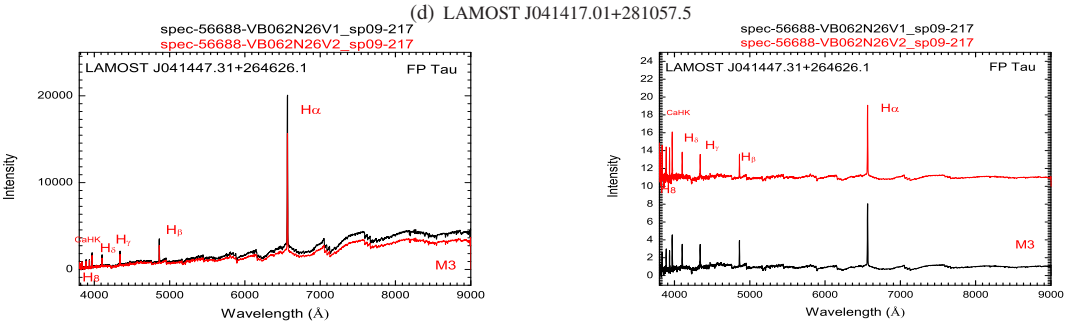

(e) LAMOST J041447.31+264626.1

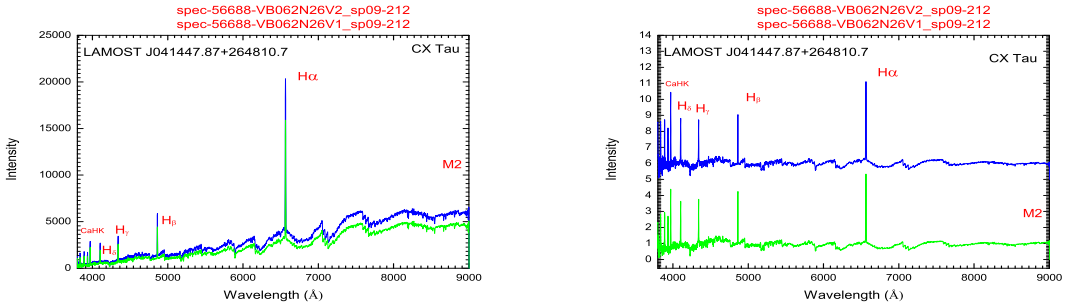

(f) LAMOST J041447.87+264810.7

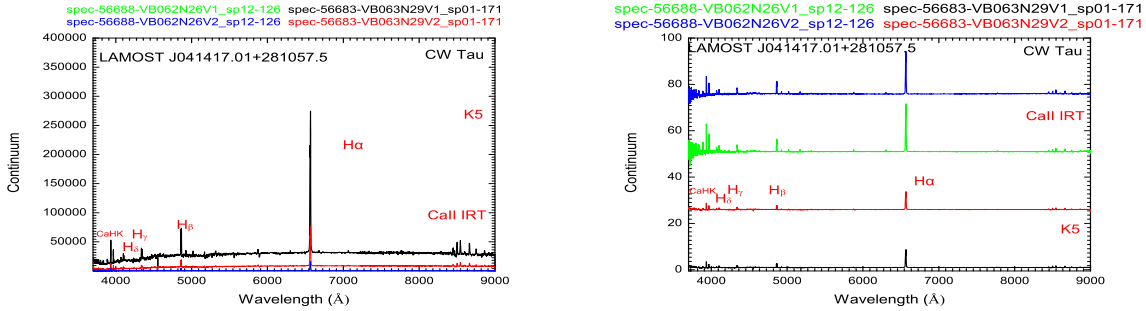

(g) LAMOST J041417.01+281057.5

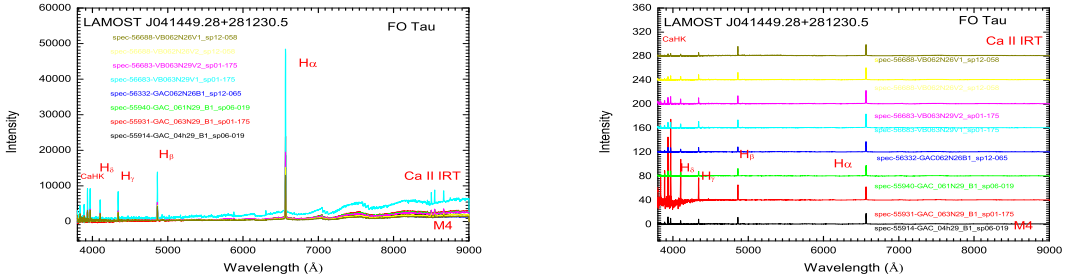

(h) LAMOST J041449.29+281230.2

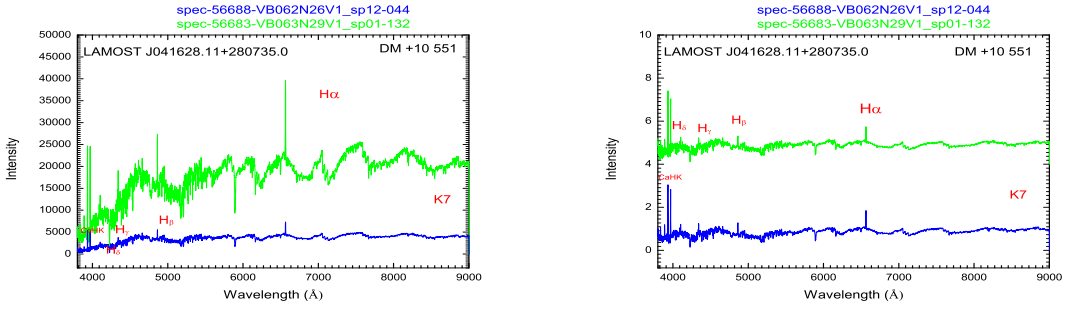

(i) LAMOST J041628.11+280735.0

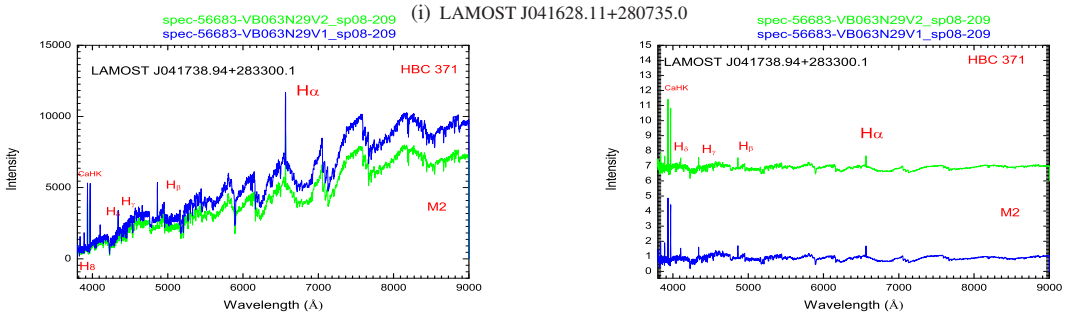

(j) LAMOST J041738.94+283300.1

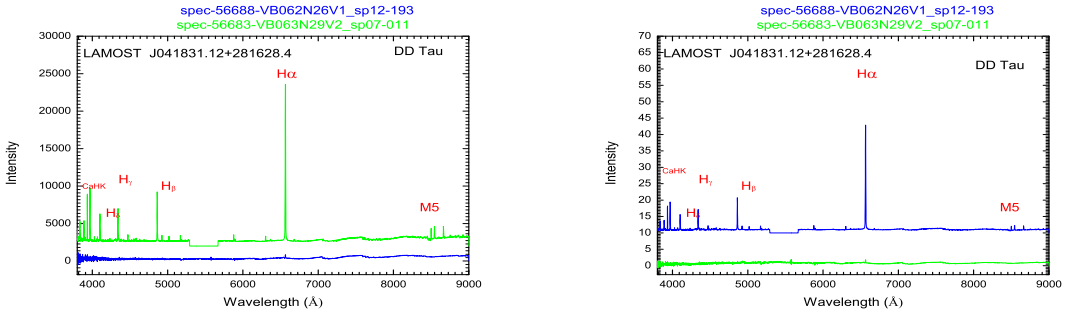

(k) LAMOST J041831.12+281628.4

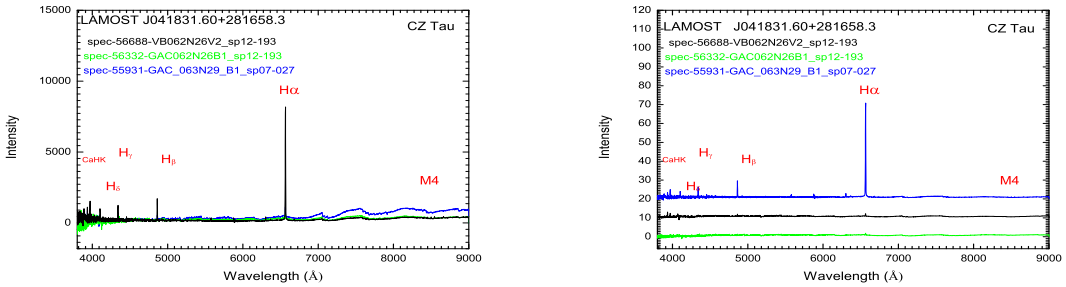

(l) LAMOST J041831.60+281658.3

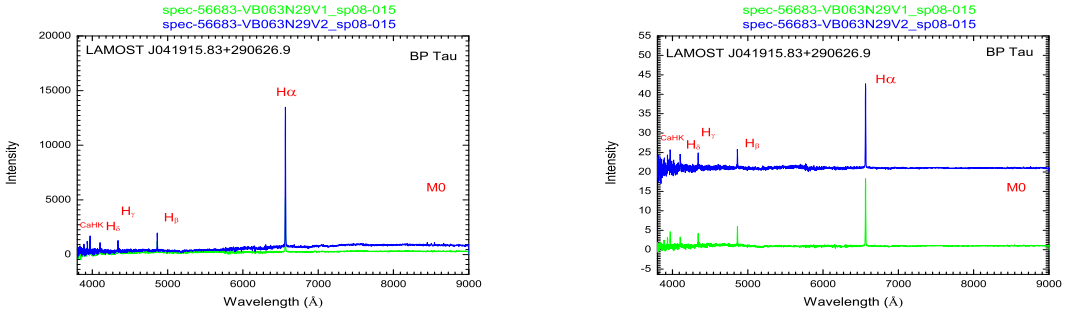

(m) LAMOST J041915.83+290626.9

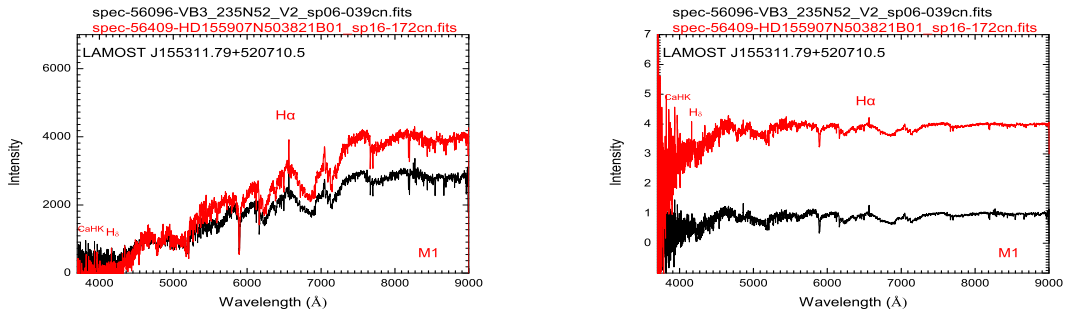

(n) LAMOST J155311.79+520710.5

Fig. 2 Examples of sources with multiple LAMOST spectra. The observed spectra are shown in the *left* panels; the continuum normalized spectra are displayed in the *right* panels. Different colors are used for spectra acquired at different times. Some of them show obvious emissions in several lines of the Ca II H&K, Hδ, Hγ, Hβ, Hα and Ca II IRT lines.

the literature (see, e.g., Fernandez et al. 1995; Kenyon & Hartmann 1995). The EWs in Hα are also similar to previous results. It is interesting to note that the criteria that we adopted could be useful for selecting new low-mass T Tau candidates in LAMOST and SDSS surveys in the future (Luhman et al. 2017). Information on the variation of radio and chromospheric activity is listed in Col. (9) and Col. (11) of Table 2, where v represents the varia-

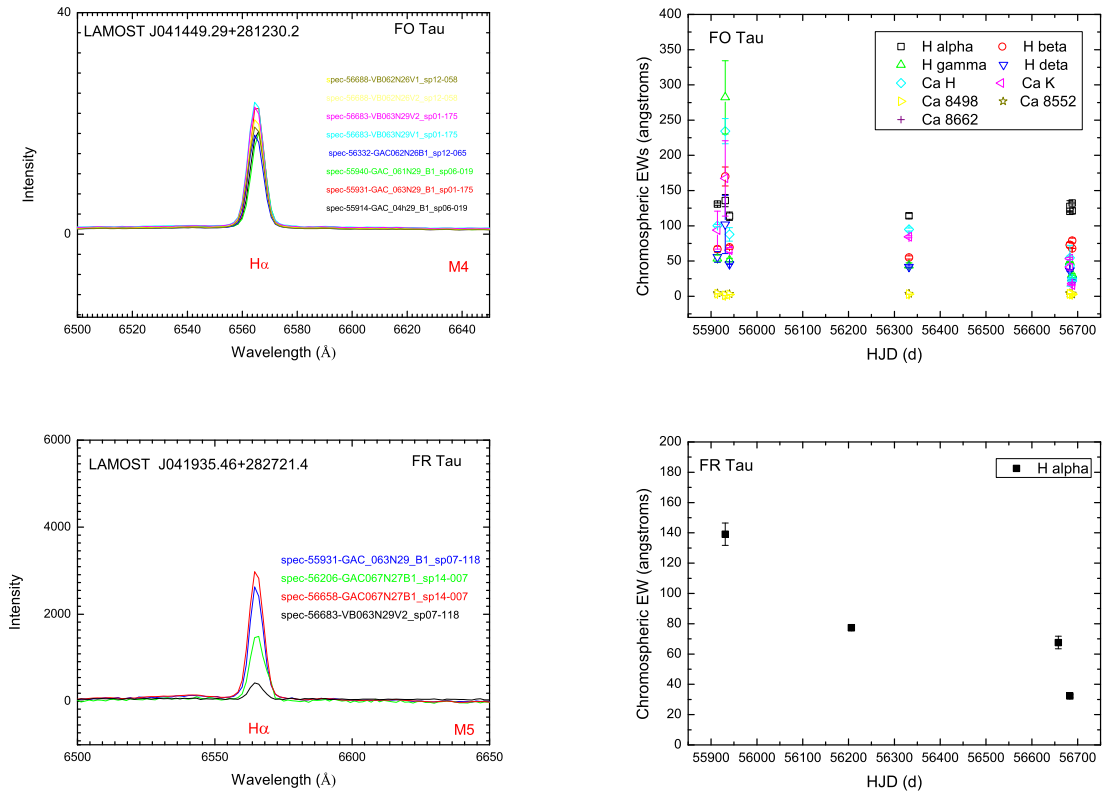

Fig. 3 Examples of spectra observed by LAMOST (*left*) and their EWs light curves (*right*) in the Hα, Hβ, Hγ, Hδ, Ca II H & K and Ca II IRT lines.

tion of radio flux ('n' means that there is no variation and '–' means that there is no data point). We regarded the peak-to-peak EW variation as an index of Hα variability. Whenever it is larger than 3 times the maximum error, we consider the object as variable and put a flag "v" in Col. (11) of Table 2 (Zhang et al. 2016). Among these stars, 28 of them show chromospheric activity variability. We plotted the LAMOST observed spectra (left) and continuum normalized spectra (right) of active objects with repeated observations and variation of activity in Figure 2. Different colors represent spectra of the same object acquired at different times. We also plotted some examples of the observed spectra and their EW light curves in the Hα, Hβ, Hγ, Hδ, Ca II H&K and Ca II IRT lines in Figure 3.

A variation of line intensity is clearly displayed by Figure 3. The EW variation might be due to the variation of chromospheric activity or accretion over the star surfaces. From the values of EWs, there is variation on a long-term scale of a year shown by FO Tau and FR Tau. These variations might be caused by accretion over the star surfaces. Indeed FO Tau and FR Tau (Andrews & Williams 2005; Wichmann et al. 1996; Furlan et al. 2011; Luhman et al. 2010, 2017) possess a strong infrared excess which classifies them as classical T Tau stars with thick and dense circum-stellar disks and likely strong mass accretion onto the central star from the disk. An even more interesting point to note is that there is simultaneous radio and chromospheric activity for several objects. The observed radio emission exhibited variability on timescales of minutes to days in the 8–12 GHz radio light curves for dwarf nova type cataclysmic variables stars U Gem (Coppejans et al. 2016). The T Tau S source displays variable radio emission (Johnston et al. 2004). Several objects show both radio flux and chromospheric activity variability. We plotted the objects with radio and chromospheric variability in Figure 4, where the LAMOST observed spectra are on the left side and the continuum normalized spectra on the right.

4.2 Chromospheric Activity Properties in the Ca II IRT Lines

The Ca II IRT lines are very important chromospheric indicators, which are formed in the low chromosphere (e.g., Montes et al. 2000; Zhang et al. 2015). In our sam-

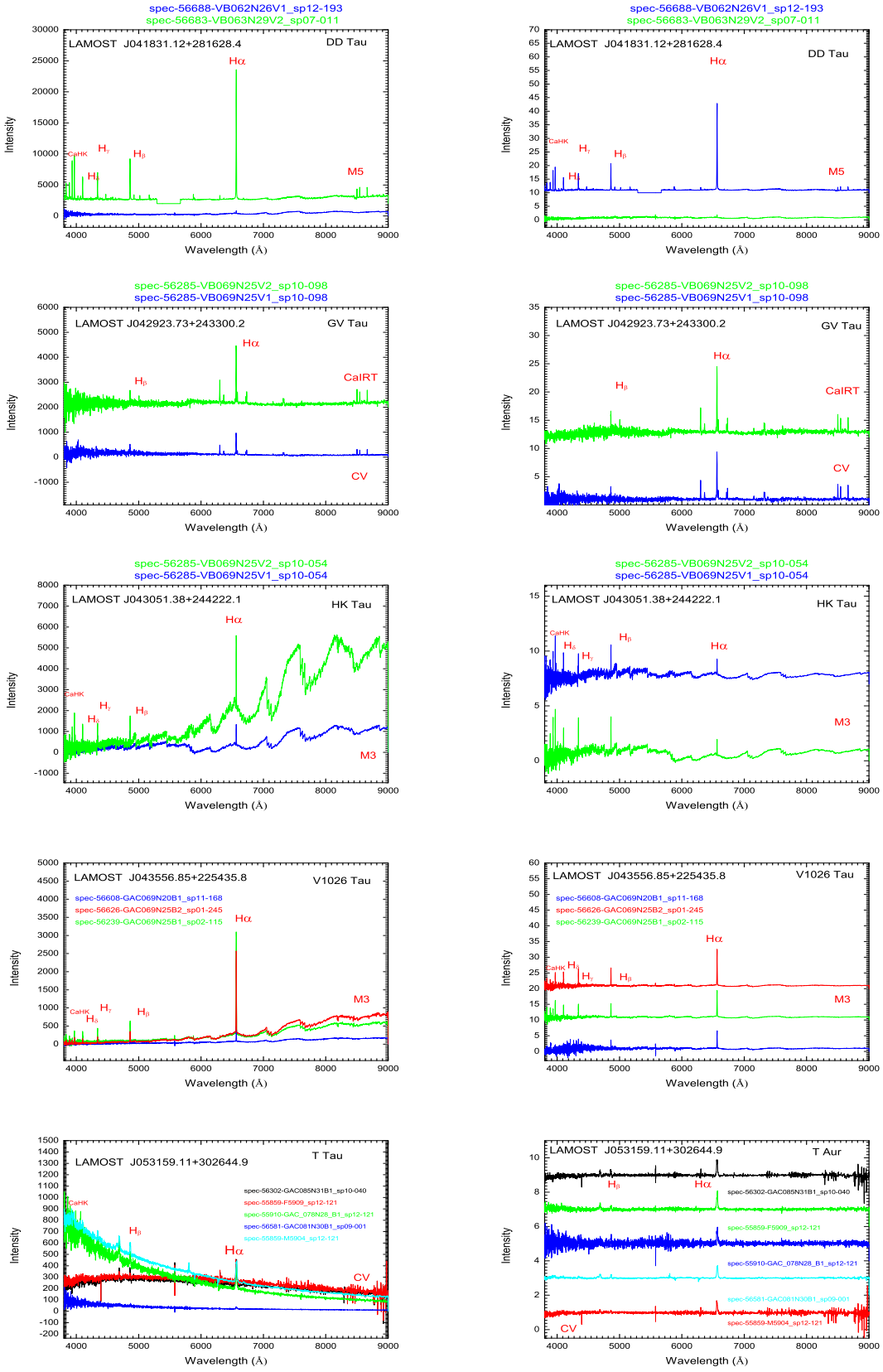

Fig. 4 Observed LAMOST spectra of radio stars with variation in both radio flux and chromospheric activity.

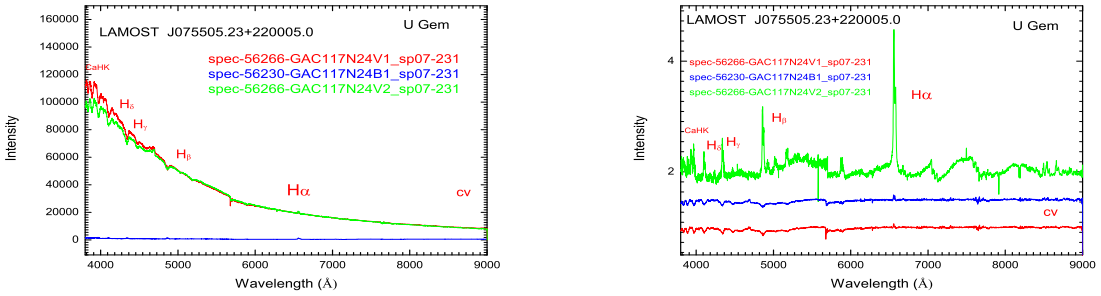

Fig. 4 — *Continued.*

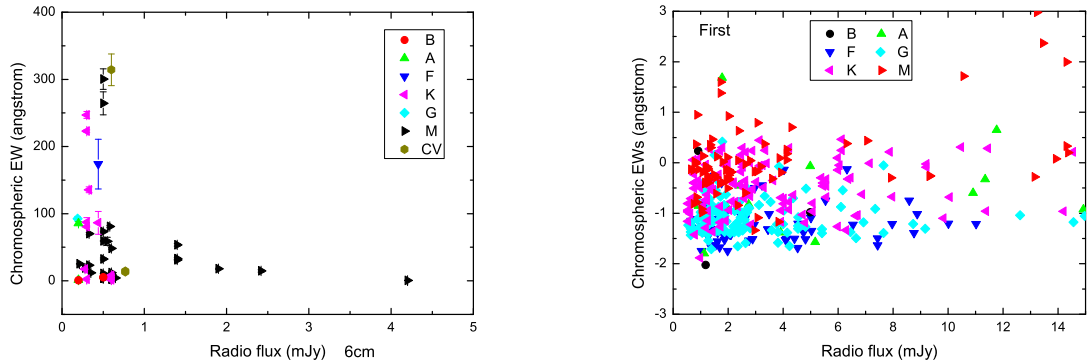

Fig. 5 Relationship between observed EWs of chromospheric activity indicators in the Hα line and radio flux of radio stars.

ple there are 14 radio stars with Ca II IRT emission lines in Table 3.

We list their relevant parameters: the number (Col. (1)), LAMOST name (Col. (2)), spectral type (Col. (3)), the reference (Col. (4)), other name (Col. (5)), EWs of three Ca II IRT lines (Col. (6) to Col. (8)), and the EW_{8542}/EW_{8498} ratio (Col. (9)) in Table 3.

The data indicate that these 14 radio stars have strong chromospheric activity emission. There have been many studies carried out on chromospheric activity in the Ca II IRT lines, Ca II H&K lines, and the Hα, Hβ and other hydrogen lines using the subtraction technique of non-active templates (e.g., Montes et al. 2000; Busà et al. 2007; Frasca et al. 2011, 2016; Pi et al. 2016). We believe more active objects can be detected if the subtraction technique is applied, and many active objects are missing without considering the spectral subtraction. The stars with pure emission in the Ca II IRT lines have a low effective temperature and, as a consequence, a low photospheric flux, which makes the line show emission. Eventually, they can be strong accretors. We hope to find more objects with strong emission in the Ca II IRT lines and determine their statistical properties in the future. The value of the ratio EW_{8542}/EW_{8498} is also an indicator of the optical thickness of the emitting plasma, which is helpful for distinguishing between stellar plages and prominences (see, e.g., Herbig & Soderblom 1980; Landman 1980). Our values of EW_{8542}/EW_{8498} for the 14 radio stars fall mostly within the range 0.4–1.8 and are listed in the Col. (9) of Table 3. These small values mean that the chromospheric activity comes from optically thick emissions in probable stellar plage regions. These low ratios were also associated with several radio stars (e.g., Arévalo et al. 1999; Zhang et al. 2016).

4.3 Relationship between Chromospheric Activity and Radio Flux

Magnetic fields in the stellar interior produce chromospheric plages and coronal radio emissions. For different types of active stars, such as RS CVn systems (e.g., Fraquelli 1978; Su et al. 1994) and dMe stars (e.g., Gudel et al. 1989, Osten et al. 2005), flare events have been detected using a combination of radio continuum, optical photometry, and optical, ultraviolet and X-ray spectro-

scopic observations. Radio outbursts may be preceded by Hα enhancement (e.g., Fraquelli 1978). There might be a correlation between strong chromospheric plages and strong flares in radio wavelengths. To examine the relationship between chromospheric activity and radio flux, we plot the chromospheric EWs of the Hα line, and the radio flux at 21 cm of radio stars from the FIRST survey (right), as well as the chromospheric EWs in the Hα line, and the radio flux at 6 cm of radio stars in Figure 5 (left) (e.g., Wendker 1995). Different symbols represent the results of different spectral types. As can be seen from Figure 5, there is no obvious trend in the chromospheric emission and radio coronal flux. The most likely reason for this behavior is that the observations at optical and radio wavelengths were not simultaneous and the sources are strongly variable. The radio flux, for instance, can go from a few mJy in a quiescent stage to several hundred mJy during flares, with timescales for bursts ranging from a few hours to a few days (e.g., Umana et al. 1995).

5 SUMMARY

We analyzed 783 good stellar spectra for 610 radio stars by mining the LAMOST spectroscopic survey DR2. Using the EWs of the Hα line, we detected 89 objects with emission above the Hα continuum in 147 spectra. There are 36 objects with repeated observations, 28 of which show chromospheric activity variability. Furthermore, we found 14 radio stars showing emissions in the Ca II IRT lines. This is the first catalog of radio stars observed in the LAMOST spectral survey. In the future, LAMOST will observe more radio stars, and we will update this catalog of radio stars. These new data will help us to address the study of activity variation at optical and radio wavelengths and their relation on better statistical grounds.

Acknowledgements This work is supported by the Joint Research Fund in Astronomy (U1631236, U1431114, U1631109 and 11263001) under cooperative agreement between NSFC and Chinese Academy of Sciences (CAS). Our paper used JHK magnitudes from the Two Micron All Sky Survey, which is a joint project of the University of Massachusetts and the Infrared Processing and Analysis Center/California Institute of Technology, funded by the National Aeronautics and Space Administration and the National Science Foundation. The Guo Shou Jing Telescope (LAMOST) is a National Major Scientific Project built by CAS. Funding for the project has been provided by the National Development and Reform Commission. LAMOST is operated and managed by NAOC, CAS.

References

Andrews, S. M., & Williams, J. P. 2005, ApJ, 631, 1134 (FO Tau)
Arévalo, M. J., & Lázaro, C., 1999, AJ, 118, 1015
Berdyugina, S. V. 2005, Living Reviews in Solar Physics, 2, 8
Berger, E. 2002, ApJ, 572, 503
Berger, E. 2006, ApJ, 648, 629
Berger, E., Basri, G., Gizis, J. E., et al. 2008, ApJ, 676, 1307
Busà, I., Aznar Cuadrado, R., Terranegra, L., Andretta, V., & Gomez, M. T. 2007, A&A, 466, 1089
Butler, C. J., Erkan, N., Budding, E., et al. 2015, MNRAS, 446, 4205
Carkner, L., Mamajek, E., Feigelson, E., et al. 1997, ApJ, 490, 735
Coppejans, D. L., Körding, E. G., Miller-Jones, J. C. A., et al. 2016, MNRAS, 463, 2229
Cui, X.-Q., Zhao, Y.-H., Chu, Y.-Q., et al. 2012, RAA (Research in Astronomy and Astrophysics), 12, 1197
Fernandez, M., Ortiz, E., Eiroa, C., & Miranda, L. F. 1995, A&AS, 114, 439
Flesch, E., & Hardcastle, M. J. 2004, A&A, 427, 387
Flesch, E. 2010, PASA, 27, 283
Flesch, E. W. 2016, PASA, 33, e052
Fraquelli, D. A. 1978, AJ, 83, 1535
Frasca, A., Fröhlich, H.-E., Bonanno, A., et al. 2011, A&A, 532, A81
Frasca, A., Molenda-Żakowicz, J., De Cat, P., et al. 2016, A&A, 594, A39
Furlan, E., Luhman, K. L., Espaillat, C., et al. 2011, ApJS, 195, 3
Güdel, M. 2002, ARA&A, 40, 217
Gudel, M., Benz, A. O., Bastian, T. S., et al. 1989, A&A, 220, L5
Gunn, J. E., Carr, M., Rockosi, C., et al. 1998, AJ, 116, 3040
Hall, J. C. 2008, Living Reviews in Solar Physics, 5, 2
Hawley, S. L., Covey, K. R., Knapp, G. R., et al. 2002, AJ, 123, 3409
Helfand, D. J., Schnee, S., Becker, R. H., White, R. L., & McMahon, R. G. 1999, AJ, 117, 1568
Helfand, D. J., White, R. L., & Becker, R. H. 2015, ApJ, 801, 26
Herbig, G. H., & Soderblom, D. R. 1980, ApJ, 242, 628
Hilton, E. J., West, A. A., Hawley, S. L., & Kowalski, A. F. 2010, AJ, 140, 1402
Hughes, V. A. 1988, ApJ, 333, 788
Ivezić, Ž., Menou, K., Knapp, G. R., et al. 2002, AJ, 124, 2364
Johnston, K. J., Fey, A. L., Gaume, R. A., et al. 2004, ApJ, 604, L65
Karoff, C., Knudsen, M. F., De Cat, P., et al. 2016, Nature Communications, 7, 11058

Kenyon, S. J., & Hartmann, L. 1995, ApJS, 101, 117
Kimball, A. E., Knapp, G. R., Ivezić, Ž., et al. 2009, ApJ, 701, 535
Landman, D. A. 1980, ApJ, 237, 988
Luhman, K. L., Allen, P. R., Espaillat, C., Hartmann, L., & Calvet, N. 2010, ApJS, 186, 111
Luhman, K. L., Mamajek, E. E., Shukla, S. J., & Loutrel, N. P. 2017, AJ, 153, 46
Luo, A.-L., Zhao, Y.-H., Zhao, G., et al. 2015, RAA (Research in Astronomy and Astrophysics), 15, 1095
McLean, M., Berger, E., & Reiners, A. 2012, ApJ, 746, 23
McMahon, R. G., White, R. L., Helfand, D. J., & Becker, R. H. 2002, ApJS, 143, 1
Mohanty, S., Jayawardhana, R., & Basri, G. 2005, ApJ, 626, 498
Montes, D., Fernández-Figueroa, M. J., De Castro, E., et al. 2000, A&AS, 146, 103
Nguyen, D. C., Brandeker, A., van Kerkwijk, M. H., & Jayawardhana, R. 2012, ApJ, 745, 119
Osten, R. A., Hawley, S. L., Allred, J. C., Johns-Krull, C. M., & Roark, C. 2005, ApJ, 621, 398
Osten, R. A., Hawley, S. L., Allred, J., et al. 2006, ApJ, 647, 1349
Paredes, J. M. 2005, in EAS Publications Series, 15, EAS Publications Series, eds. L. I. Gurvits, S. Frey, & S. Rawlings, 187
Pi, Q. F., Zhang, L. Y., Chang, L., et al., 2016, RAA (Research in Astronomy and Astrophysics), 16, 153
Skrutskie, M. F., Cutri, R. M., Stiening, R., et al. 2006, AJ, 131, 1163
Su, B.-M., Mutel, R. L., Li, Y.-S., & Zhang, F.-J. 1994, Chinese Astronomy and Astrophysics, 18, 11
Umana, G., Trigilio, C., Tumino, M., Catalano, S., & Rodono, M. 1995, A&A, 298, 143
Wang, S.-G., Su, D.-Q., Chu, Y.-Q., Cui, X., & Wang, Y.-N. 1996, Appl. Opt., 35, 5155
Wendker, H. J. 1987, A&AS, 69, 87
Wendker, H. J. 1995, A&AS, 109, 177
Wendker, H. J. 2015, VizieR Online Data Catalog, 8099
West, A. A., Hawley, S. L., Walkowicz, L. M., et al. 2004, AJ, 128, 426
West, A. A., Morgan, D. P., Bochanski, J. J., et al. 2011, AJ, 141, 97
White, S. M., Jackson, P. D., & Kundu, M. R. 1989, ApJS, 71, 895
Wichmann, R., Krautter, J., Schmitt, J. H. M. M., et al. 1996, A&A, 312, 439
Wu, Y., Luo, A.-L., Li, H.-N., et al. 2011, RAA (Research in Astronomy and Astrophysics), 11, 924
Wu, Y., Luo, A., Du, B., & Guo, Y. 2014, in IAU Symposium, 298, Setting the Scene for Gaia and LAMOST, eds. S. Feltzing, G. Zhao, N. A. Walton, & P. Whitelock, 445
Yi, Z., Luo, A., Song, Y., et al. 2014, AJ, 147, 33
York, D. G., Adelman, J., Anderson, Jr., J. E., et al. 2000, AJ, 120, 1579
Zhang, L.-Y., & Gu, S.-H. 2008, A&A, 487, 709
Zhang, L., Pi, Q., & Zhu, Z. Z. 2015, RAA (Research in Astronomy and Astrophysics), 15, 252
Zhang, L., Pi, Q., Han, X. L., et al. 2016, New Astron., 44, 66
Zhao, G., Zhao, Y.-H., Chu, Y.-Q., Jing, Y.-P., & Deng, L.-C. 2012, RAA (Research in Astronomy and Astrophysics), 12, 723